Dynamical Model Compensation for Near-Earth Satellite Orbit Determination

KENNETH A. MYERS*
Aerospace Research Laboratories, Wright-Patterson Air Force Base, Ohio
AND
BYRON D. TAPLEY†
The University of Texas at Austin, Austin, Texas

Operational requirements in modern space applications often demand orbit determination accuracies which are limited by fundamental mathematical and computational restrictions. It is shown in realistic computer simulation studies how these difficulties can be alleviated for typical near-Earth satellites by employing dynamical model compensation (DMC) and accurate observations in the extended Kalman filter. Unmodeled and unknown accelerations affecting the motion of the satellite are effectively compensated by treating them as a first-order, Gauss-Markov stochastic process. Although conventional state noise compensation (SNC) can provide satisfactory results for many applications, the DMC method offers a significant increase in estimation accuracy. Numerical behavior of the DMC structure is summarized as a function of a priori statistical parameters to aid in filter design analyses for operational applications.

Introduction

OPERATIONAL methods in orbit determination have progressed from deterministic methods, used during the early years of the space program, to least squares and differential correction techniques,[1] still widely used today, to sequential filtering and smoothing schemes, the subject of much current research.[2] Well proven techniques in batch processing or even deterministic methods may suffice for some operations; however, they can be inadequate (especially for on-line operation) in many modern and sophisticated missions, where accuracy requirements are specified in terms of meters and arc-seconds. In some cases, such as precision pointing control missions and geophysical applications, the orbit determination problem may well become a limiting factor in mission success. There exists an inherent mathematical equivalence between the more conventional batch and the relatively newer sequential processing techniques, but the latter techniques usually converge more rapidly and provide more accurate estimates when used in their extended form with state noise compensation.[3]

Higher accuracy requirements are accompanied by a need for more precise mathematical models for prediction of the spacecraft position and velocity. In conflict with this need, however, are limitations imposed not only by an abbreviated knowledge of the true forces acting on the spacecraft but also by computational considerations, such as computation time, storage, and round-off error. For instance, current geopotential models[4] provide spherical harmonic coefficients up to degree 22 and order 16; dynamical atmospheric density models[5] provide for seasonal-latitudinal variations, diurnal and geomagnetic effects, etc. However, the necessary storage for programs which utilize these models and the computer time required for the numerical integrations is often prohibitive. Regardless of the sophistication of the mathematical model, there will always be unknown forces acting on the spacecraft due to tidal forces, variations in solar radiation pressure, vehicle outgassing, and so forth ad infinitum. As a consequence, the differential equations used to describe the satellite motion will be subject to model errors.

This paper describes an approach which is intended to offset the fundamental limitations of model accuracy and computational load. The method utilizes accurate observational data in conjunction with a filter algorithm designed to compensate for the unknown or neglected components of the dynamical model. A wide variety of dynamical model error compensation techniques has appeared in the literature[7]; they can usually be classified as either adaptive or non-adaptive. The non-adaptive methods are based on a priori modifications to the filter structure and are primarily intended to maintain the state covariance (or the Kalman gain) at some suitable level for sustained filter operation. Although most of these techniques require little additional computational effort, the results are dependent upon a priori knowledge of the model error. On the other hand, adaptive methods are designed to adjust the dynamical model so as to improve the filter operation during the estimation process. These methods usually demand a significant increase in computational effort, but they often provide more optimal estimates in the sense of improved "local" estimation accuracy.

Of the non-adaptive techniques, the most common, and probably the simplest to implement, is the state noise compensation (SNC) algorithm.[2] This method treats the unmodeled dynamical effects as a white noise process. The over-all effect of this assumption is to provide a lower bound, represented by the integrated state noise contribution Q, on the predicted state covariance $\bar{P}$; however, the value of Q must be determined from a priori considerations and is usually assumed to remain constant throughout the estimation. In another non-adaptive method,[8] the propagated state covariance is scaled by an appropriate factor s which preserves filter sensitivity to the new observations. An approach by Schmidt[9] sensitizes the filter to more recent observations by introducing either an additive gain term or a scalar correction factor in the Kalman gain. A "limited memory" filter proposed by Jazwinski[10] discards old data and bases successive estimates on a "batch" of the last N observations. Finally, the Schmidt-Kalman filter[10] treats the case in which certain identifiable portions of the dynamical model are poorly known; by including this uncertainty in the filter algorithm, a

Received May 23, 1974. Revision received August 15, 1974. This research was sponsored in part by AFOSR Grant 72-2233 and the Air Force Institute of Technology. Views expressed in this report are those of the authors and do not necessarily reflect those of the U.S. Air Force.

Index categories: Navigation, Control, and Guidance Theory; Spacecraft Tracking.

* Captain, U.S. Air Force, Applied Mathematics Research Laboratory. Member AIAA.

† Chairman and Professor, Department of Aerospace Engineering and Engineering Mechanics. Member AIAA.

steady-state lower bound is maintained on the covariance. The non-adaptive techniques proposed in these references are concerned primarily with the prevention of divergence and do not attack its fundamental cause.

The adaptive techniques can be further classified as "structural" and "statistical" methods. The latter category includes maximum likelihood or Bayesian estimators[11] which provide an estimate of the state noise covariance matrix simultaneously with the system state; these methods are studied in Ref. 12 for the orbit determination problem. This investigation is restricted to the "structural" methods, which are designed to adaptively estimate the true value of the unmodeled acceleration along with the state. In this approach, the unknown functional expression that governs the neglected dynamics is approximated by an assumed, time-correlated dynamical structure; the adaptive qualities of this technique are further enhanced by estimating those parameters which characterize the assumed structure. Advantages of this approach are as follows: 1) an estimate of the model error permits better "local" estimation of the state; 2) an estimate of the unmodeled dynamical structure enhances state prediction capability; 3) the basic filter algorithm is unaltered; and, 4) the unknown acceleration estimate can be used in post-flight analyses to improve the basic dynamical model. Disadvantages of the method are: 1) the a priori state covariance $\hat{P}_o$ and noise statistics (a Q matrix) must be determined for parameters in the assumed structure; and, 2) the state vector dimension must be increased to incorporate the assumed structure parameters.

The assumed dynamical structure is largely a matter of design choice, and of course no single choice could be expected to perform well in all applications. Typical structures have ranged from simple constants[13] to high-order differential equations.[14] One of the most effective approaches, due to Tapley and Ingram,[15] treats the unmodeled acceleration as a first-order, Gauss-Markov (or Ornstein-Uhlenbeck) stochastic process. This structure has been successfully applied in lunar orbit determination problems. Higher order Gauss-Markov processes and other dynamical structures have proven successful in low-thrust interplanetary navigation studies by Hagar[7] and Eller.[16] In this paper, the first-order, Gauss-Markov structure is applied in the orbit determination problem for typical near-Earth satellites. Particular emphasis is given to the effects of realistic dynamical model errors and changing observation geometry and density. The accuracy of the estimates of both the state and unmodeled acceleration is evaluated through numerical simulations.

Description of Simulations

Simulation results for this investigation were obtained on the CDC 6600 digital computer at the University of Texas at Austin. Observations are generated in the program from a set of true equations of motion and are corrupted by the addition of white, Gaussian noise. An extended Kalman filter is used for estimating the true spacecraft state vector based on the simulated observations. Translational equations of motion for the spacecraft are expressed in an Earth-centered, inertial (ECI) coordinate system, where the X-Y plane lies in the Earth equatorial plane with the X- and Z- axes directed to the mean equinox and north pole, respectively. The simulated real-world equations of motion are integrated with an efficient Runge-Kutta-Fehlberg algorithm. When the spacecraft is in view of a tracking station, a fourth-order algorithm is used with fixed stepsize equal to the observation interval; when no observations are available, the spacecraft state is propagated with a variable stepsize, eighth-order algorithm. The equations of motion include the acceleration of the Earth's gravitational field $\bar{\mathbf{a}}_g$, two-body perturbations of the sun and moon $\bar{\mathbf{a}}_p$, and atmospheric drag $\bar{\mathbf{a}}_d$, i.e.,

$$\ddot{\bar{\mathbf{r}}} = \bar{\mathbf{a}}_g + \bar{\mathbf{a}}_p + \bar{\mathbf{a}}_d \tag{1}$$

where $\bar{\mathbf{r}}$ is the simulated true position vector in the ECI system. The expression for the gravitational acceleration $\bar{\mathbf{a}}_g$ is taken from the 1968 JPL geopotential model[17] which includes spherical harmonic terms up to degree 6 and order 4. The luni-solar perturbation[1] is

$$\bar{\mathbf{a}}_p = \mu_m \left\{ \frac{\bar{\mathbf{r}}_m - \bar{\mathbf{r}}}{|\bar{\mathbf{r}}_m - \bar{\mathbf{r}}|^3} - \frac{\bar{\mathbf{r}}_m}{\mathbf{r}_m^3} \right\} + \mu_s \left\{ \frac{\bar{\mathbf{r}}_s - \bar{\mathbf{r}}}{|\bar{\mathbf{r}}_s - \bar{\mathbf{r}}|^3} - \frac{\bar{\mathbf{r}}_s}{\mathbf{r}_s^3} \right\} \tag{2}$$

where μ_m and μ_s represent gravitational parameters and $\bar{\mathbf{r}}_m$ and $\bar{\mathbf{r}}_s$ are position vectors of the moon and sun, respectively, in the ECI coordinate system. Drag acceleration is obtained from the relation

$$\bar{\mathbf{a}}_d = -\tfrac{1}{2} B_c \rho v \bar{\mathbf{v}} \tag{3}$$

where the density ρ is given by,[18]

$$\rho = \rho_o \left[\frac{a}{a + b(h - h_o)} \right]^{1/b} \text{ kg/m}^3 \tag{4}$$

and the constants are: $a = 16.4$ km; $b = 0.232$; $\rho_o = 3.951 \times 10^{-9}$ kg/m^3; and, $h_o = 140$ km. The variable h is altitude in kilometers, and the ballistic coefficient is $B_c = 0.01$ m^2/kg.

Perturbing acceleration for the filter-world equations of motion includes only the effect of Earth oblateness (J_2), i.e.,

$$\ddot{\bar{\mathbf{r}}} = \nabla U \tag{5}$$

where the potential function U is,

$$U = \tfrac{1}{2} \mu_e \frac{J_2 R_e^2}{\mathbf{r}^3} \left\{ 1 - 3 \frac{Z^2}{\mathbf{r}^2} \right\} \tag{6}$$

R_e is the Earth radius, μ_e the gravitational parameter, and J_2 the second harmonic coefficient.[17] This provides a reasonable mismatch between the filter-world and real-world models, which is necessary to evaluate filter performance in the presence of dynamical model errors. Furthermore, the inclusion of J_2 in the filter-world model is necessary for effective estimation in the near-earth orbit determination problem considered here, so the adopted model closely represents the "minimum" computational requirement for the filter. During prediction phases of the simulations (when the satellite is out of view of the tracking stations) filtered estimates are propagated with the real-world dynamical model defined by Eq. (1).

Radar range ρ and doppler range-rate $\dot{\rho}$ observations are made from each of twelve land-based tracking stations. Standard deviations in the range and range-rate measurements are $\sigma_\rho = 5$ m and $\sigma_{\dot{\rho}} = 0.005$ m/sec, respectively, employed both for generation of the true observations and estimation of the state. Range and range-rate observations are conducted simultaneously at five-second intervals. Tracking station locations[19] (Table 1) are defined in an earth-fixed coordinate system, aligned with the ECI coordinate system XYZ at $t_o = 0$, which rotates about the Z-axis due to rotation of the earth. Perfect knowledge is assumed for both the station locations and the filter-world, observation-state model.

Two orbital configurations were selected: Case 1 is a low-altitude, eccentric orbit with a perigee/apogee height of 160/380 kilometers, an inclination of 110°, argument of perigee of 130°, and orbital period of 90 min; and, Case 2 is a higher 940-km alt, near-circular orbit with an inclination of 100° and an orbital period of 104 min. Initial state vector for the true simulated orbits and the sun and moon are presented in Table 2. The initial nominal state estimate error is 100 meters and 1 m/sec in each component of position and velocity, respectively. The initial a priori state covariance is a diagonal matrix with standard deviations of 1000 m and 10 m/sec in the position and velocity elements, respectively. Simulations are started with the satellite positioned near its ascending node crossing at about 50° longitude west of Greenwich. A summary of the tracking station schedule is provided in Table 1.

Simulation results are presented in terms of the root-sum-square (rss) position error ΔR and the estimated position covariance norm N_R. An estimate of the average true error over the estimation interval, from step j (shortly after initial convergence) to step k, is provided by an error performance (EP) factor

Table 1 Tracking station locations and observation schedule

Station location	East longitude (deg.)	Latitude (deg.)	Elevation (m)	Case 1 observation schedule (min.)	Case 2 observation schedule (min.)
Trinidad	298.5	11.0	245	0–8, 89–93	0–12, 99–112
Antigua	298.0	17.0	−27	0–9, 90–94	0–14, 101–114
Eglin AFB	273.8	30.5	45	10–11, 93–101	7–17, 104–120
New Hampshire	288.4	42.9	211	8–16, 98–100	6–22, 108–120
Cold Lake	250.0	54.5	654	15–20, 101–108	14–27, 113–120
Clear	210.9	64.2	240	20–25, 107–110	20–34
Shemya	174.2	52.7	93	27–28	27–38
Guam	144.9	13.6	161	No observations	42–51
Carnarvon	113.7	−24.9	1	47–53	50–67
Antarctica	60.0	−66.5	100	60–67	65–80
Santiago	289.3	−33.1	727	80–85	89–102
Vandenberg AFB	239.5	34.8	305	No observations	113–120

$$EP_R \equiv \sum_{i=j}^{k} \Delta R_i \Delta t_i \Big/ \sum_{i=j}^{k} \Delta t_i \tag{7}$$

where Δt_i is the integration stepsize and ΔR_i is the true position rss error computed at the ith step. Likewise, a qualitative covariance performance (CP) factor is defined as

$$CP_R \equiv \sum_{i=j}^{k} [N_{R_i} - \Delta R_i]\Delta t_i \Big/ \sum_{i=j}^{k} \Delta t_i \tag{8}$$

Similar definitions are employed for the velocity error performance (EP_V) and covariance performance (CP_V) factors. The CP factors should be positive when the estimated covariances provide reasonably good bounds on the estimation errors.

The Filter Algorithm

The sequential estimation algorithm is the extended Kalman filter (EKF), probably the most practical and most widely used filter in current nonlinear applications.[10] The basic formulation is reviewed as follows. Evolution of the true nonlinear dynamical process is assumed to be governed by the system of first-order differential equations

$$\dot{X} = F(X,t) + u(t);\ X(t_o) = X_o \tag{9}$$

where X is an n-dimensional state vector, F is a known function (model) of the state variables, and $u(t)$ is an n-vector of state noise with the following statistical properties: $E[u(t)] = 0$; $E[u(t)u^T(s)] = U(t)\delta(t-s)$; and, $E[u(t)X_o^T] = 0$. The state noise covariance $U(t)$ is an $n \times n$ matrix, and $\delta(t-s)$ is the Dirac delta function. Since the true state can never be known exactly, it must be estimated by making observations Y_i, a p-vector, at discrete times t_i, as follows,

$$Y_i = G(X_i, t_i) + v_i;\ i = 1, 2, \ldots, k-1 \tag{10}$$

The v_i is a p-vector of observation errors which is assumed to have the properties: $E[v_i] = 0$; $E[v_i v_j^T] = R_i \delta_{ij}$; and, $E[X(t_i)v_j^T] = 0$. The observation noise covariance R_i is a constant $p \times p$ matrix, and δ_{ij} is the Kronecker delta. In addition to the observations, an a priori estimate of the state, $\hat{X}_{k-1}$, is provided at time t_{k-1} along with an associated $n \times n$ conditional covariance matrix,

$$\hat{P}_{k-1} = E[(X_{k-1} - \hat{X}_{k-1})(X_{k-1} - \hat{X}_{k-1})^T | Y_{k-1}] \tag{11}$$

where Y_{k-1} implies conditioning on all observations from Y_1 through Y_{k-1}.

Given the previous a priori information, the predicted state estimate $\bar{X}_k$ is obtained by integrating the following system of nonlinear differential equations from t_{k-1} to t_k,

$$\dot{\bar{X}} = F(\bar{X}, t);\ \bar{X}(t_{k-1}) = \hat{X}_{k-1} \tag{12}$$

where the bar indicates a nominal, predicted value. The predicted state covariance is given by the relation

$$\bar{P}_k = \Phi(k, k-1)\hat{P}_{k-1}\Phi^T(k, k-1) + Q_{k-1} \tag{13}$$

where

$$Q_{k-1} = \int_{t_{k-1}}^{t_k} \Phi(t_k, \tau)U(\tau)\Phi^T(t_k, \tau)\, d\tau \tag{14}$$

is the integrated form of the state noise covariance contribution to $\bar{P}_k$. The familiar state transition matrix $\Phi(t, t_{k-1})$ is obtained by integrating the following $n \times n$ system of differential equations from t_{k-1} to t_k,

$$\dot{\Phi}(t, t_{k-1}) = A(t)\Phi(t, t_{k-1});\ \Phi(t_{k-1}, t_{k-1}) = I_{n \times n} \tag{15}$$

where

$$A(t) \equiv \left.\frac{\partial F(X,t)}{\partial X}\right|_{\bar{X}(t)} \tag{16}$$

is an $n \times n$ matrix of partial derivatives evaluated on the current best estimate of the state $\bar{X}(t)$.

Now, given a new observation Y_k at time t_k, an approximate (to within first-order) minimum variance, unbiased estimate of the state is given by

$$\hat{X}_k = \bar{X}_k + K_k[Y_k - G(\bar{X}_k, t_k)] \tag{17}$$

where K_k is the $n \times p$ "Kalman gain" matrix

$$K_k = \bar{P}_k H_k^T [H_k \bar{P}_k H_k^T + R_K]^{-1} \tag{18}$$

and

$$H_k \equiv \left.\frac{\partial G(X_k, t_k)}{\partial X}\right|_{\bar{X}_k} \tag{19}$$

is a $p \times n$ matrix of partial derivatives evaluated on the predicted state estimate $\bar{X}_k$. Finally, a first-order estimate for the a posteriori covariance of the state estimate is provided by

$$\hat{P}_k = [I - K_k H_k]\bar{P}_k \tag{20}$$

Table 2 Initial orbital elements and state vectors

Initial true state vector	Case 1	Case 2	Sun	Moon
X_o (km)	6720.0367196	7283.4000000	−9.5565264376E07	3.1984176728E05
Y_o (km)	−23.718370095	0.0	1.0822774989E08	1.8224301020E05
Z_o (km)	65.165686263	0.0	4.6931172218E07	1.0464866207E05
U_o (km/sec)	−0.1789464900	0.0	−2.2659335006E01	−0.6031532716E00
V_o (km/sec)	−2.6195551497	−1.2878209354	−1.7107589543E01	0.7312020610E00
W_o (km/sec)	7.1971686229	7.3035954578	−7.4182486699E00	0.3892105127E00

SNC Results

In the non-adaptive technique of state noise compensation (SNC), the true dynamical equations of motion represented by Eq. (9) are assumed to be of the form

$$\begin{aligned} \dot{r} &= v \\ \dot{v} &= a_m(r, v, t) + w(t) \end{aligned} \tag{21}$$

where $X^T(t) \equiv [r^T : v^T]$, and r and v are 3-vectors of the true position and velocity; a_m is a 3-vector function of acceleration components to be employed in the filter-world model (due only to the primary two-body attraction and J_2); and, $w(t)$ is a 3-vector white, Gaussian noise process with zero mean and covariance $W \equiv \sigma_w{}^2 I_{3\times 3}$. The nominal or filter-world model in Eq. (12) is governed by the corresponding system

$$\begin{aligned} \dot{\bar{r}} &= \bar{v} \\ \dot{\bar{v}} &= a_m(\bar{r}, \bar{v}, t) \end{aligned} \tag{22}$$

An analytic expression for the integrated state noise contribution in Eq. (14) is given by[12]

$$Q_{k-1} = \begin{bmatrix} \frac{1}{3}\delta_k{}^3 W & \vdots & \frac{1}{2}\delta_k{}^2 W \\ \cdots & \cdots & \cdots \\ \frac{1}{2}\delta_k{}^2 W & \vdots & \delta_k W \end{bmatrix} \tag{23}$$

where the observation interval, $\delta_k \equiv t_k - t_{k-1}$, is assumed to be constant and sufficiently small to satisfy stationarity conditions on the noise process $w(t)$. Note that Q_{k-1} (or σ_w) must be selected to "cover" the effects of computational errors, neglected nonlinearities, unmodeled accelerations due to zonal harmonics above J_2 (up to degree 6) and tesseral harmonics to order 4, atmospheric drag, and the two-body attraction of the sun and moon. During prediction periods, it is assumed that no model errors are present, and Q_{k-1} is set equal to the null matrix.

A plot of the true rss position error ΔR and covariance norm N_R is presented for the SNC method in Figs. 1 and 2 for the two orbit determination test cases. The rss error curve has a jagged appearance, due to the random character of successive state estimates; however, the curve becomes smooth during periods of prediction, when no tracking stations are observing the satellite. The smoother curve, usually bounding the rss errors, is the estimated state covariance norm, which grows during prediction phases and drops sharply when new observations become available. Best over-all performance was obtained with the following values of $\sigma_w{}^2$: for Case 1, 2×10^{-5} m^2/sec^4; and for Case 2, 2×10^{-6} m^2/sec^4. As shown in Table 3, for example, the average rss position error in Case 1 was 27.31 m; on the average, the estimated covariance provided a conservative bound or "margin of error" of 18.97 m on the position estimation error.

Table 3 Comparison of EP and CP factors for SNC vs DMC methods

Case	Method	EP_R (m)	CP_R (m)	EP_V (m/sec)	CP_V (m/sec)
1	SNC	2.731E+01	1.897E+01	6.318E−02	5.834E−02
2	SNC	9.530E+00	3.680E+00	2.491E−02	9.133E−03
1	DMC	1.913E+01	6.568E+01	4.806E−02	2.145E−01
2	DMC	1.296E+01	4.684E+00	2.914E−02	1.781E−02

Plots for both test cases display acceptable estimation results. The covariance estimates provide a reliable measure of the true error, even during the prediction phases. After initial filter convergence, the estimation errors become small (on the order of one meter error in position); during this period, the satellite passes over the North American continent, where usually two or more tracking stations are making simultaneous observations. Toward the middle of the estimation interval, as the satellite descends into the Southern Hemisphere, fewer observations are available, and errors typically grow to 10 or 20 m in position when only one station views the satellite. During observation coverage gaps, the errors grow to as much as 150 m in Case 1 and 50 meters in Case 2. Errors are again sharply reduced when the satellite passes over North America after a full orbit.

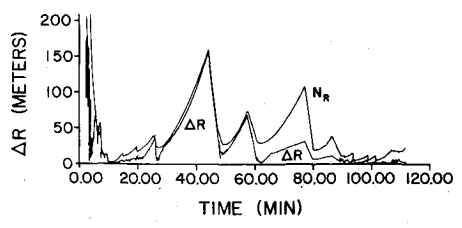

Fig. 1 Case 1 position error and covariance for SNC method.

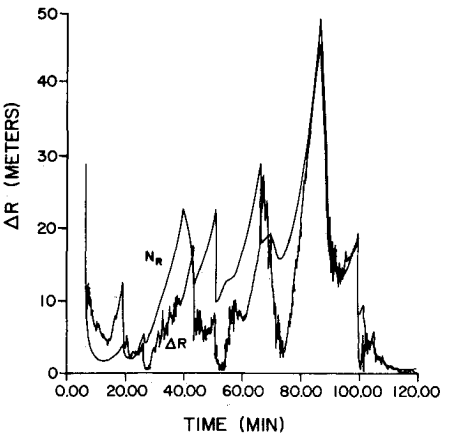

Fig. 2 Case 2 position error and covariance for SNC method.

Three special runs were conducted to investigate certain model error effects for near-Earth satellites. First, when $\sigma_w = 0$ the true error increased rapidly to large values, while the covariance estimate asymptotically approached zero; obviously, the presence of state noise aids considerably in preventing filter divergence. Secondly, when the filter-world model includes only the two-body effect of the earth, the true errors grossly exceed the covariance estimate, with position errors reaching values of 12 km. On the other hand, if a perfect filter-world model (equivalent to the simulation real-world model) is used significantly accurate results can be obtained; errors are uniformly bounded by the estimated covariance, even during prediction, at values less than about 2 or 3 m.

DMC Results

The true equations of motion for a general dynamical system can be expressed as a system of first-order differential equations,

$$\begin{aligned} \dot{r} &= v \\ \dot{v} &= a_m(r, v, t) + a_u(t) \end{aligned} \tag{24}$$

where $a_u(t)$ represents a 3-vector of all unknown and/or unmodeled acceleration components, which may be either deterministic or stochastic in nature. It would be desirable to use the true functional form of $a_u(t)$, but this is seldom feasible from a computational standpoint. Furthermore, $a_u(t)$ is never completely known in practice; the best that can be done, practically speaking, is to assume a function $\varepsilon(t)$ which serves as a "good" approximation, i.e.,

$$\varepsilon(t) \cong a_u(t) \tag{25}$$

where $\varepsilon^T(t) \equiv [\varepsilon_x(t)\varepsilon_y(t)\varepsilon_z(t)]^T$. Of course, the number of possibilities for the "structure" of $\varepsilon(t)$ are unlimited, but a primary criterion is that it be computationally tractable. A common choice, $\varepsilon(t) = w(t)$, provides the SNC algorithm above. In this section, $\varepsilon(t)$ is modeled as an adaptive, time-correlated, first-order, Gauss-Markov process which satisfies the following stochastic differential equation,

$$\dot{\varepsilon}(t) = -B(t)\varepsilon(t) + u_\varepsilon(t) \tag{26}$$

The random component $u_\varepsilon(t)$ is a 3-vector of Gaussian noise with zero mean and covariance $q_\varepsilon(t)$, a diagonal matrix with elements q_{ε_x}, q_{ε_y}, q_{ε_z}, and $B(t)$ is a 3×3, diagonal matrix of the time correlation coefficients, β_x, β_y, β_z. An implicit assumption

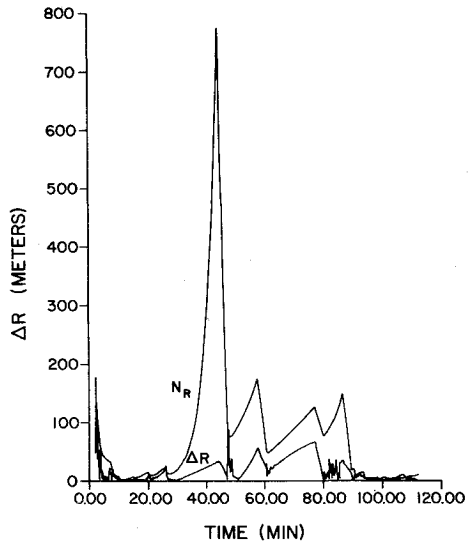

Fig. 3 Case 1 position error and covariance for DMC method.

in this structure is that the model errors ε_x, ε_y, and ε_z are uncorrelated. Further, the time correlation coefficients are unknown parameters expressed in vector form as $\beta^T(t) \equiv [\beta_x(t)\beta_y(t)\beta_z(t)]^T$. In order to maintain adaptive qualities in the algorithm, the evolution of $\beta(t)$ is assumed to be governed by the stochastic differential equation

$$\dot{\beta}(t) = u_\beta(t) \tag{27}$$

where $u_\beta(t)$ is a 3-vector of Gaussian noise with zero mean and covariance $q_\beta(t)$, a diagonal matrix with elements q_{β_x}, q_{β_y}, q_{β_z}. Thus, the true dynamical process is assumed to be governed by the following system,

$$\begin{aligned} \dot{r} &= v \\ \dot{v} &= a_m(r, v, t) + \varepsilon(t) \\ \dot{\varepsilon} &= -B\varepsilon + u_\varepsilon(t) \\ \dot{\beta} &= u_\beta(t) \end{aligned} \tag{28}$$

and the new state vector is defined by

$$X^T(t) = [r^T : v^T : \varepsilon^T : \beta^T] \tag{29}$$

The filter-world dynamical model is assumed to be of the form

$$\begin{aligned} \dot{\bar{r}} &= \bar{v} \\ \dot{\bar{v}} &= a_m(\bar{r}, \bar{v}, t) + \bar{\varepsilon}(t) \\ \dot{\bar{\varepsilon}} &= -\bar{B}\bar{\varepsilon} \\ \dot{\bar{\beta}} &= 0 \end{aligned} \tag{30}$$

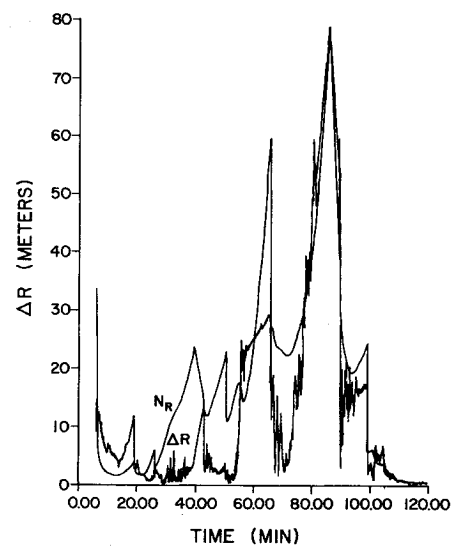

Fig. 4 Case 2 position error and covariance for DMC method.

An analytic expression[12] for the state noise contribution is given by the 12×12 matrix

$$Q_{k-1} = \begin{bmatrix} \frac{1}{4}\delta_k^4\Lambda & \frac{1}{2}\delta_k^3\Lambda & \frac{1}{2}\delta_k^2\Lambda & \phi \\ \frac{1}{2}\delta_k^3\Lambda & \delta_k^2\Lambda & \delta_k\Lambda & \phi \\ \frac{1}{2}\delta_k^2\Lambda & \delta_k\Lambda & \Lambda & \phi \\ \phi & \phi & \phi & \Upsilon \end{bmatrix} \tag{31}$$

where ϕ is the 3×3 null matrix, $\Upsilon \equiv \delta_k q_\beta$, and

$$\Lambda \equiv \begin{bmatrix} q_{\varepsilon_x}[1-e^{-2\beta_x\delta_k}]/2\beta_x & 0 & 0 \\ 0 & q_{\varepsilon_y}[1-e^{-2\beta_y\delta_k}]/2\beta_y & 0 \\ 0 & 0 & q_{\varepsilon_z}[1-e^{-2\beta_z\delta_k}]/2\beta_z \end{bmatrix} \tag{32}$$

It is assumed that all three diagonal components of q_ε and q_β are equal with standard deviations of σ_ε and σ_β, respectively. Thus, an a priori selection of the parameters σ_ε and σ_β conveniently specifies the entire state noise contribution. Of course, Q_{k-1} is set to the null matrix during prediction periods when no model errors are present.

Position estimation results for the DMC algorithm are presented for the two test cases in Figs. 3 and 4. Corresponding estimation results for the dynamical model structure are given in Figs. 5 and 6, both of which present the following information: 1) a plot of the true rss error in the estimate of the unmodeled acceleration ΔE and a superimposed plot of the unmodeled acceleration covariance estimate norm N_E; and, 2) a plot of the rss estimate of the time correlation coefficients $\Delta\beta$ with a superimposed plot of the covariance estimate norm for the time correlation coefficients N_β. Note that the "true" value of $\beta(t)$ is not determined in the simulation procedure, so the true error for this parameter cannot be determined. During

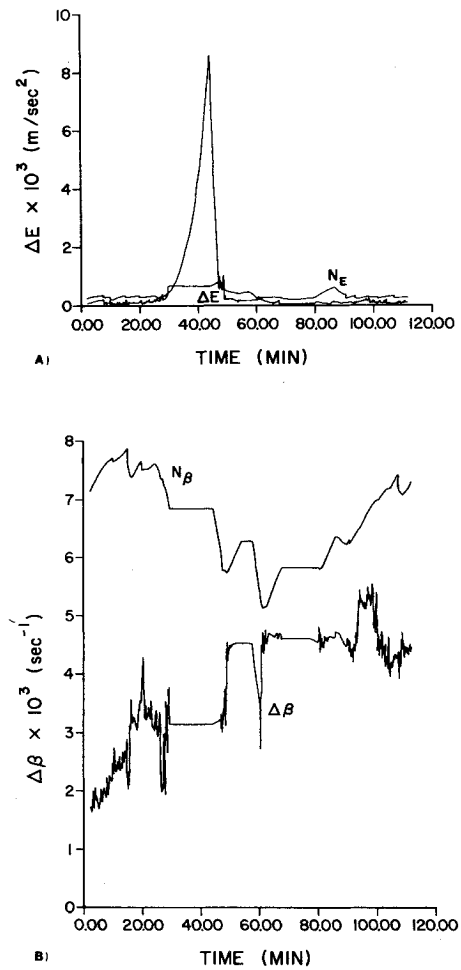

Fig. 5 DMC structure performance for Case 1. a) Unmodeled accelerations. b) Time correlation coefficients.

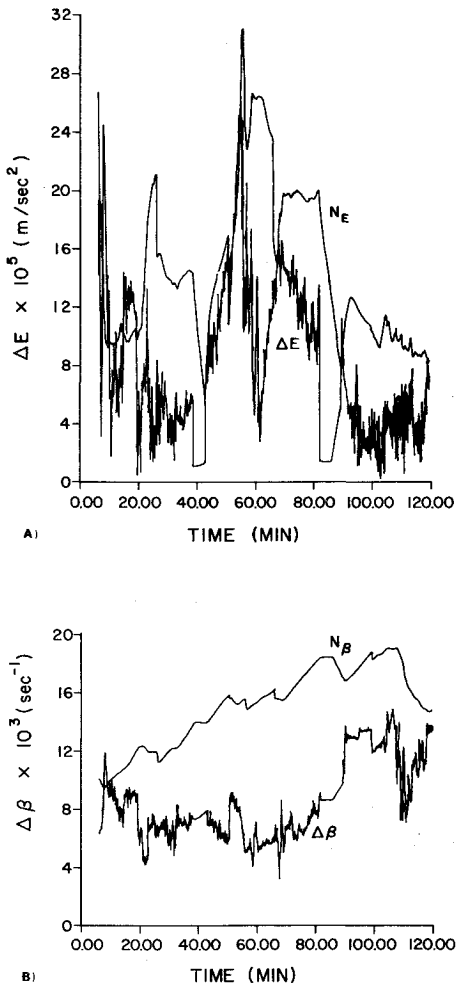

Fig. 6 DMC structure performance for Case 2. a) Unmodeled accelerations. b) Time correlation coefficients.

prediction periods, the true unmodeled acceleration drops to zero, and the last best estimate of $\varepsilon(t)$ and $\beta(t)$ is retained for initialization of the next estimation phase.

A priori statistics for the unmodeled acceleration parameters are given in Table 4. Resultant DMC estimation performance factors are compared with the SNC results in Table 3. Comparison of the plots in Figs. 3 and 4 with those for the SNC method, in Figs. 1 and 2, indicates that a dramatic improvement in estimation accuracy can be obtained with the DMC approach. The over-all average estimation error for Case 1 has been reduced from 27.3 m to 19.1 m (about 40%) in position and from 0.063 m/sec to 0.048 m/sec (about 30%) in velocity. Furthermore, it is evident that the DMC algorithm has significantly enhanced the prediction capability of the filter, as anticipated in the development. The large, 150-m prediction error at 45 min for the SNC case in Fig. 1 has been reduced to about 30 m; likewise, the 70-m prediction error at 57 min has been reduced to 50 m. However, the error at 78 min has been increased with the DMC algorithm from 30 m to about 60 m. The reason for this degradation can be seen on the component plots of $\bar{\varepsilon}(t)$, detailed in Ref. 12. It is noted that $\bar{\varepsilon}_y$ and $\bar{\varepsilon}_z$ are poorly estimated (by a single tracking station) just prior to the prediction phase, from 67 to 80 min; therefore, the position and velocity estimate becomes degraded. Evidently, the tracking period at this station is of insufficient duration to obtain a good estimate of the unmodeled acceleration prior to fade. During periods when the estimation of $\varepsilon(t)$ is good, such as the period from 5 min to about 30 min, the position and velocity estimates are significantly improved. Typically, the rss position error for the SNC method during this period is reduced by factors like "two" or "ten"; for example, at 18, 19, and 20 min the SNC errors were 6.5, 6.7, and 10.9 m, whereas the DMC errors were 2.3, 0.6, and 6.9 m, respectively. Thus, when sufficient observations are available, and when a good estimate of the unmodeled acceleration is obtained, the DMC algorithm becomes an extremely powerful estimation tool.

DMC results for Case 2 are not as impressive as for Case 1, despite the fact that more observations are available (due to higher orbital altitude). In fact, Table 3 indicates that the average over-all error in both position and velocity for the DMC method is slightly higher than that for the SNC method. Close comparison of the plots in Figs. 2 and 4, however, indicates that the larger average errors are due primarily to the larger "peak" prediction error for the DMC algorithm, i.e., the 45-m error at 85 min for the SNC method is increased to almost 80 m for the DMC method. This degradation, again, appears to be due to an insufficient number of observations just prior to the prediction interval. In other single-station tracking periods, however, the DMC outperforms the SNC method. For example, during the period from 34 to 50 min, the position errors for the SNC method exceed 6 m; whereas, the DMC method reduces these errors to less than 4 m. Specifically, at 34, 35, and 36 min the SNC position errors are 6.6, 7.5, and 7.1 m, whereas the DMC errors are 0.7, 1.2, and 2.4 m, respectively. Similar comments apply to the velocity estimates. Another factor which probably contributes to a poorer demonstration of the DMC method in Case 2 is the magnitude of the unmodeled acceleration itself. Components of the unmodeled acceleration in Case 1, due to large drag forces, reach values three to five times higher than those in Case 2. As one might expect, estimation of the unmodeled acceleration plays an increasingly effective role in filter performance as the true unmodeled acceleration increases.

Table 4 A priori statistics for the DMC structure parameters

Case	ε_o (m/sec^2)	β_o (sec^{-1})	$P_{o_\varepsilon}^{1/2}$ (m/sec^2)	$P_{o_\beta}^{1/2}$ (sec^{-1})	σ_ε (m/sec^3)	$\sigma_\beta \delta_k^{1/2}$ (sec^{-1})
1	0.0	1E−03	5E−05	4E−03	1.5E−05	2E−04
2	0.0	1E−03	1E−03	5E−03	8.0E−06	5E−04

Numerical Character of the DMC Structure

The DMC algorithm appears to be well suited for operational, on-line use in the orbit determination problem, but its success in a given application is dependent upon simulation studies for proper determination of the a priori statistics. As a result of experience obtained in this study, a number of important factors were discovered with regard to "selection" of these parameters and their influence on the estimation results. These points are summarized as an aid for other filter design studies.

1) Estimation of the time correlation coefficients $\beta(t)$ was found to be far more effective than estimation of the time constants defined by $T^T(t) \equiv [T_x\ T_y\ T_z]^T$, where, for example, $T_x \equiv 1/\beta_x$, and the differential equation for $T(t)$ is specified as

$$\dot{T}(t) = 0 \tag{33}$$

It was found that estimated covariance elements associated with $T(t)$ ranged from about 10^4 to 10^6 sec^2. Therefore, the state covariance matrix, which contains numbers like 10^{-2} for position elements, 10^{-6} for velocity elements, and 10^{-8} for unmodeled acceleration elements, tended to have poor numerical conditioning. Use of $\beta(t)$ provides numbers like 10^{-6}, which is much more consistent with other elements of the covariance matrix.

2) Initial conditions for the nominal Gauss-Markov differential equations are somewhat influential on the estimation results. The initial value of the unmodeled acceleration ε_o is less critical than that for the time correlation β_o; in fact, $\varepsilon_o \equiv 0$ seemed to provide as good a result as any. On the other hand, it was found that $\beta_o \equiv 0$ was a very ineffective choice, and that best results were obtained with values like 10^{-3} or 10^{-4} sec^{-1} which are comparable to the estimated values of $\beta(t)$ in the problem.

In addition, the value of β_o should be related to its initial variance P_{o_β}, as described in the next paragraph.

3) A priori standard deviations for the unmodeled acceleration parameters, $P_{o_\varepsilon}{}^{1/2}$ and $P_{o_\beta}{}^{1/2}$, should be chosen only slightly larger than the true values of $\varepsilon_o(t)$ and $\beta_o(t)$. The value of $P_{o_\varepsilon}{}^{1/2}$, less critical than $P_{o_\beta}{}^{1/2}$, is reduced by the initial observations somewhat rapidly, like the estimates of the position and velocity covariances. On the other hand, $P_\beta{}^{1/2}$ changes very slowly, initially. Due to the diagonal form of the initial covariance P_o and null elements associated with $\beta(t)$ in the observation geometry matrix $H(t)$, the lower right, 3×3 submatrix of $KH\bar{P}$ is null, and the estimated covariance $\hat{P}$ remains unchanged in the elements associated with $\beta(t)$ until the off-diagonal elements of $\hat{P}$ begin to "fill in." The initial value P_{o_β} should be chosen about a factor of five greater than the initial value β_o. If P_{o_β} is too large, it takes many observations (since $\beta(t)$ is poorly observable) to bring P_β down to its proper value, e.g. half an orbit of tracking data. On the other hand, if P_{o_β} is too small the estimation of $\beta(t)$ quickly diverges, both P_β and $\beta(t)$ reach a constant value, and the estimate of $\varepsilon(t)$ loses its time-correlated, adaptive qualities.

4) Previous formulations[15] of the DMC algorithm have propagated $T(t)$ as a constant in Eq. (33); whereas, in this development, $\beta(t)$ is "driven" by a white noise process in Eq. (27). It was found that if $\beta(t)$ is treated as a constant, estimation of the unmodeled acceleration parameters rapidly diverges; P_β decreases to a very small value, and $\beta(t)$ approaches a constant, providing no adaptive input to the algorithm. Thus, the use of "forcing noise" in the estimation of $\beta(t)$ was found to be absolutely mandatory in this application. Furthermore, the "amount" of noise, embedded in σ_β, is a critical factor, as explained next.

5) The noise variances σ_ε and σ_β were found to be the most influential a priori parameters in the algorithm. In simulation testing, it is easiest to determine a good value of σ_ε by inspection of superimposed plots of the true unmodeled acceleration error and estimated covariance, such as those in Figs. 5a and 6a. If σ_ε is too small, the estimation of $\varepsilon(t)$ (and position and velocity) quickly diverges, with the true estimation error of $\varepsilon(t)$ exceeding the covariance bound. More subtle effects can occur if σ_ε is chosen too large; in this case, not only is the covariance bound raised to an unnecessarily large value, permitting larger errors in the estimate of $\varepsilon(t)$, but also the estimation of $\beta(t)$ is "washed out." Thus, a large amount of forcing noise $u_\varepsilon(t)$ tends to "hide" the adaptive effects of $\beta(t)$ in the differential equation for $\varepsilon(t)$; variations in the estimate of $\beta(t)$ and P_β become suppressed and appear to have a divergent character. The parameter σ_β plays an inportant role in "maintaining" an adaptive estimate of $\varepsilon(t)$. Elements of the state transition matrix $\Phi(t, t_{k-1})$ which are associated with $\beta(t)$ essentially provide a direct mapping (identity matrix) of P_β in the propagation relationship, Eq. (13). Thus, P_β changes only by an amount $\Upsilon = \sigma_\beta{}^2 \Delta t$ during the propagation. Since the estimation of P_β involves a subtraction (of the positive quantity $KH\bar{P}$) σ_β must be selected to "return" P_β to an appropriate value at each propagation time. If σ_β is chosen too small, P_β approaches a small value, and the estimation of $\beta(t)$ becomes divergent; on the other hand, if σ_β is too large the estimate of P_β climbs, somewhat linearly, in an unbounded manner. Thus, a good value of σ_β is obtained when the estimation of P_β appears to be fluctuating with a steady-state nature. This type of behavior in P_β produces a sustained, although somewhat random, adaptive estimate of $\beta(t)$, as illustrated on the rss plots of $\beta(t)$ in Figs. 5b and 6b.

Conclusions

The simulation results obtained in this study indicate that the SNC algorithm, a simple extended Kalman filter with a constant state noise covariance matrix, should provide acceptable estimation results for many near-Earth satellite applications, despite large dynamical model errors. However, a significant improvement in estimation accuracy should be possible with the DMC algorithm. During periods of sparse observations or poor observation geometry, the estimate of the unmodeled acceleration can deteriorate, but degradation in the position and velocity estimate appears to be of small consequence; and, when the estimate of the unmodeled acceleration is good, superior filter performance can be obtained. As a final note, it is stressed that only one DMC structure has been investigated. It is conceivable that other structures, such as a second-order Gauss-Markov process, could provide even better estimation results.

References

[1] Escobal, P. R., *Methods of Orbit Determination*, Wiley, New York, 1965.

[2] Leondes, C. T., ed., *Theory and Applications of Kalman Filtering*, NATO AGARDograph 139, Technical Editing and Reproduction, Ltd., London, Feb., 1970. (Reproduced by National Technical Information Service, Springfield, Va.).

[3] Schutz, B. E., McMillan, J. D., and Tapley, B. D., "A Comparison of Estimation Methods for the Reduction of Laser Observations of a Near-Earth Satellite," Vail, Colo., July 1973.

[4] Lerch, F. J., "Gravitational Field Models for the Earth (GEM 1 & 2)," X-553-72-146, May 1972, Goddard Space Flight Center, Greenbelt, Md.

[5] Jacchia, L. G., Special Rept. 332, May 1971, Smithsonian Astrophysical Observatory, Washington, D.C.

[6] Schlee, S. F., Standish, C. J., and Toda, N. F., "Divergence in the Kalman Filter," *AIAA Journal*, Vol. 5, No. 6, June 1967, pp. 1114–1120.

[7] Hagar, H., Jr., "Model Error Compensation Techniques for Linear Filtering," AMRL Rept. 1055, Aug. 1973, Applied Mechanics Research Lab., The University of Texas at Austin, Austin, Tex.

[8] Tarn, T. J., and Zaborszky, J., "A Practical, Nondiverging Filter," *AIAA Journal*, Vol. 8, No. 6, June 1970, pp. 1127–1133.

[9] Schmidt, S. F., "Estimation of State with Acceptable Accuracy Constraints," Interim Rept. No. 67-4, Jan. 1967, Analytical Mechanics Associates, Inc., Lanham, Mass.

[10] Jazwinski, A. H., *Stochastic Processes and Filtering Theory*, Academic Press, New York, 1970.

[11] Weiss, I. M., "A Survey of Discrete Kalman-Bucy Filtering with Unknown Noise Covariances," *AIAA Guidance, Control, and Flight Mechanics Conference*, Santa Barbara, Calif., Aug., 1970.

[12] Myers, K. A., "Filtering Theory Methods and Applications to the Orbit Determination Problem for Near-Earth Satellites," AMRL Rept. 1058, Nov. 1973, Applied Mechanics Research Lab., The University of Texas at Austin, Austin, Tex.

[13] Curkendall, D. W., "Problems in Estimation Theory with Applications to Orbit Determination," UCLA-ENG-7275, Sept. 1972, School of Engineering and Applied Science, UCLA, Los Angeles, Calif.

[14] Carpenter, G. C., and Pitkin, E. T., "Orbit Determination for a Thrusted Space Vehicle," AIAA Paper 69-901, Princeton, N.J., 1969.

[15] Tapley, B. D. and Ingram, D. S., "Orbit Determination in the Presence of Unmodeled Accelerations," *IEEE Trans. on Automatic Control*, Vol. AC-18, Aug. 1973, pp. 364–373.

[16] Eller, T. J., "Sequential Estimation of Random Thrust Errors for Solar Electric Propulsion Spacecraft," AMRL Rept. 1057, Dec. 1973, Applied Mechanics Research Laboratory, The University of Texas at Austin.

[17] Melbourne, W. G., et al., "Constants and Related Information for Astrodynamic Calculations, 1968," TR 32-1306, July 15, 1968, Jet Propulsion Lab., California Institute of Technology, Pasadena, Calif.

[18] Gura, I. A., Abbott, A. S., and Hendrickson, H. T., "Configuration Studies for Autonomous Satellite Navigation," Rept. TR-0059 (6784)-1, May 1971, The Aerospace Corp., El Segundo, Calif.

[19] Marsh, J. G., et al., "A Unified Set of Tracking Station Coordinates Derived from Geodetic Satellite Tracking Data," Tech. Rept. X-553-71-370, July 1971, Goddard Space Flight Center, Greenbelt, Md.